SSRG International Journal of Electrical and Electronics Engineering
ISSN: 2348-8379 / https://doi.org/10.14445/23488379/IJEEE-V10I2P118

Volume 10 Issue 2, 196-206, February 2023

Original Article

Circularly Polarized Antenna for C and X-Band Applications using Characteristic Mode Analysis

Vamshi Kollipara[1], V. Siva Nagaraju[2], M. Krishnaiah[3], M. Thirupathi[4], A. Ushasree[5], Naluguru Udaya Kumar[6], Samineni Peddakrishna[1*]

[1]*School of Electronics Engineering, VIT-AP University, Amaravati, India.*
[2]*Department of ECE, Institute of Aeronautical Engineering, Hyderabad, India.*
[3]*Department of ECE, Vidya Jyothi Institute of Technology, Hyderabad, India.*
[4]*Department of ECE, St. Martin's Engineering College, Secunderabad, India.*
[5]*Department of ECE, Gokaraju Rangaraju Institute of Engineering and Technology, Hyderabad, India.*
[6]*Department of ECE, Marri Laxman Reddy Institute of Technology and Management, Hyderabad, India.*

[1*]*Corresponding Author: krishna.samineni@gmail.com*

Received: 12 January 2023 Revised: 12 February 2023 Accepted: 21 February 2023 Published: 28 February 2023

Abstract - *This article describes a coplanar waveguide (CPW) feed inverted L- strip slot antenna implementation along with characteristic mode analysis (CMA) to obtain circular polarization (CP) with broad bandwidth. The antenna design includes a microstrip feed annular ring patch and an inverted L-strip asymmetric square slot. The resonant and radiating behavior of the inverted L-strip with asymmetric square slot are analyzed using CMA for the first six characteristic modes (CMs) to attain CP. The annular ring microstrip-fed patch is then excited based on the CMs response to achieve broadband CP. To further assess the accuracy of the simulation results, a prototype is fabricated on a single-layered FR-4 substrate measuring 25×25 mm^2. Upon measurement, the antenna displays an S_{11} less than -10 dB of 59.6% (5.50 - 10.17 GHz) impedance bandwidth and 3dB circular polarization of 46.8% (5.98 - 9.64 GHz) axial ratio bandwidth. The proposed antenna's operating bandwidth may include the satellite and naval radar required for military applications.*

Keywords - *Antenna, Broadband, Circular polarization, Characteristic modes, Characteristic mode analysis.*

1. Introduction

The present-day surge in the usage of wireless, mobile, and satellite communication technologies has resulted in an amplified requirement for dual-band, multi-band, or broadband antennas in ultra-wideband (UWB) applications [1-3]. Circularly polarized (CP) antennas are necessary as they offer a solution to the issues associated with linear polarization (LP) that are associated such as Faraday Rotation, interferences due to multipath, and polarization mismatch between the transmitter and receiver [4-5]. In order to achieve circular polarization, a combination of two modes that are 90 degrees to each other and have uniform amplitude is utilized.

In literature, numerous approaches have been described to achieve CP, including diagonal feeding, rectangular patch with different slots and stubs, truncating edges, asymmetric radiators, crossed-shaped apertures, and array configurations with either single-feed or dual-feed options [6-14]. Although single-feed CP antennas are compact and straightforward to manufacture, they have a restricted bandwidth, especially in terms of their 3dB axial ratio (AR) bandwidth, which has been a drawback. To address this issue, dual-feed CP antennas have been designed. These antennas are fed at two distinct points, resulting in a 90^0-phase difference in two perpendicular directions. However, these antennas are bulky and complex in structure and are typically designed using full-wave modeling and optimization with little physical insight. The absence of physical understanding in the design process can complicate the antenna shape and feeding optimization and result in deceptive simulated current distributions. To address this issue, characteristic mode analysis (CMA) has recently garnered significant attention from researchers, as it provides source-free techniques to understand the antenna's natural resonance properties [15-20]. A profound understanding of how the antenna operates on a physical level can generate valuable modal analysis outcomes that guide optimization efforts, achieving the required radiation performance at a particular frequency. CMA is a versatile analysis that can improve bandwidth, polarization, and structure optimization.

This research paper introduces a new CP antenna geometry that uses CM analysis to optimize the antenna's resonance behavior. To excite the antenna on a 0.4mm FR-4 substrate, a microstrip feed with an annular ring is utilized.

Several antenna parameters are assessed, including AR, reflection coefficient, gain, and radiation patterns. The antenna's performance is scrutinized through experimental validation by measuring these parameters. This antenna provides extensive circular polarization and can cover both the uplink frequency of the C-band and X-band military uplink and downlink frequencies.

2. Characteristic Mode Theory

This section provides an overview of modal analysis and a substantial role in antenna design. Modal analysis was first introduced by Garbacz [36] and was later developed by Turpin [22]. They presented a unique set of characteristic modes (CMs) for any arbitrary perfect electric conductor (PEC) that is independent of any particular source. Harington and Mautz [38] further improved the idea by relating the surface current to its tangential electric field. The main idea behind modal analysis is to extract resonant frequencies of fundamental and higher-order modes and electromagnetic structure properties such as modal current and radiation behavior for each mode in the far-field zone.

By understanding the modal behavior of the antenna geometry, the radiation performance at a specific frequency can be optimized [24,37]. Modal analysis can be mathematically considered an eigenvalue (EV) analysis, and its characteristic modes can be obtained from equation (1). This approach provides a powerful technique for optimizing antenna performance by enabling researchers to gain an intuition of the natural resonance properties and determine the necessary radiation performance at a given frequency.

$$X(\overrightarrow{Jn}) = \lambda n R(\overrightarrow{Jn}) \quad (1)$$

Where The EV is denoted by a symbolλn, while the eigenfunctions (Eigen currents) are denoted by $\overrightarrow{Jn}$, The operator $R$is real and X is imaginary impedance. According to equation (1), the characteristic modes $(\overrightarrow{Jn})$ are defined as actual currents on the conductive body. The shape and size of the body are the only factors that determine these currents, and any particular source or excitation does not influence them. From equation (1), the EV equation (2) is formulated from the method of moment impedance matrix.

$$[X][I]_n = \lambda n[R][I]_n \quad (2)$$

The concept of EV analysis and using characteristic modes to obtain natural resonance information of each mode index. The EV equation (1) represents the characteristic current, where n is the mode index. The EV equation gives the mode information at different frequencies based on the stored energy on the radiating surface. The modes are classified as resonant mode, inductive mode, and capacitive mode based on the stored energy (electric and magnetic) at various frequencies. However, discriminating higher-order modes using EV becomes difficult at higher frequencies as they are closely grouped. To address this difficulty, modal significance (MS) and characteristic angle (CA) can be used to analyze other parameters derived from the EV. These characteristics and parameters examine all aspects of the radiation capacity of specific modes. MS, in particular, determines the significant modes for a particular design and can be defined using equation (3).

$$MS = \frac{1}{|1+J\lambda_n|} \quad (3)$$

The MS calculation involves determining the modal contribution to the far field. The mode with the highest MS is considered the dominant mode. The MS provides the resonant frequency and bandwidth of the modes contributing significantly to the antenna. Furthermore, the characteristic angle determines the direction of maximum radiation for each mode. By analyzing these parameters, it is possible to optimize the antenna's radiation performance and bandwidth for specific applications. Therefore, using CMs in modal analysis provides physical insight into the antenna's behavior and facilitates the optimization of antenna design.

The other parameter, CA, is useful for identifying phase lag between the surface current and tangential electric field. This can be defined in equation (4).

$$\phi_n = 180^0 - tan^{-1}(\lambda_n) \quad (4)$$

The CA information can be used to estimate the phase angle between two orthogonal modes, which is very useful for generating CP radiation. To generate CP radiation in antenna design, it excites equal amplitude orthogonal modes with quadrature (90°) phase difference concurrently. This can be simultaneously observed from MS and CA and current modal distribution.

2.1. Proposed Design Modal Analysis

The CMs of an inverted L-strip design with an asymmetric square slot have been conducted using CMA. The proposed design analysis begins from a simple square patch without any substrate, as depicted in Fig. 1, with a dimension of 25 × 25 mm^2. Fig. 2 depicts the MS and CA for the initial six modes of Patch #1. As observed from Fig. 2, the first two degenerated modes (Mode 1 and Mode 2) resonate at 6.43 GHz, and Mode 4 resonates at 7.35 GHz. However, these modes are irrelevant to generating CP for quadrature phase shifts. Also, the other modes depicted in Fig.2 are insignificant in the specified band. Therefore, the basic patch antenna is modified with different levels of modifications to attain quadrature phase shift for CP radiation and reduce the resonance frequency of higher-order modes.

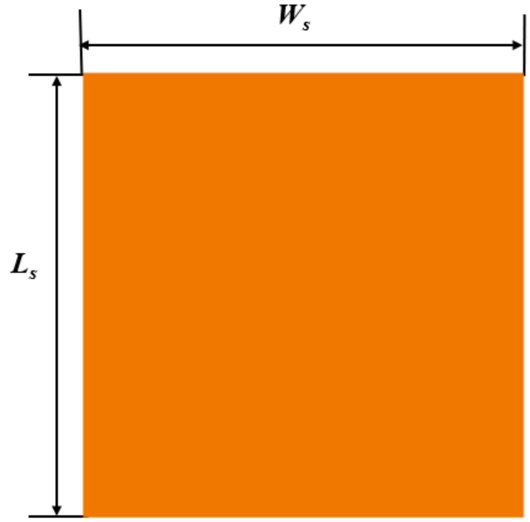

Fig. 1 Symmetric square patch #1

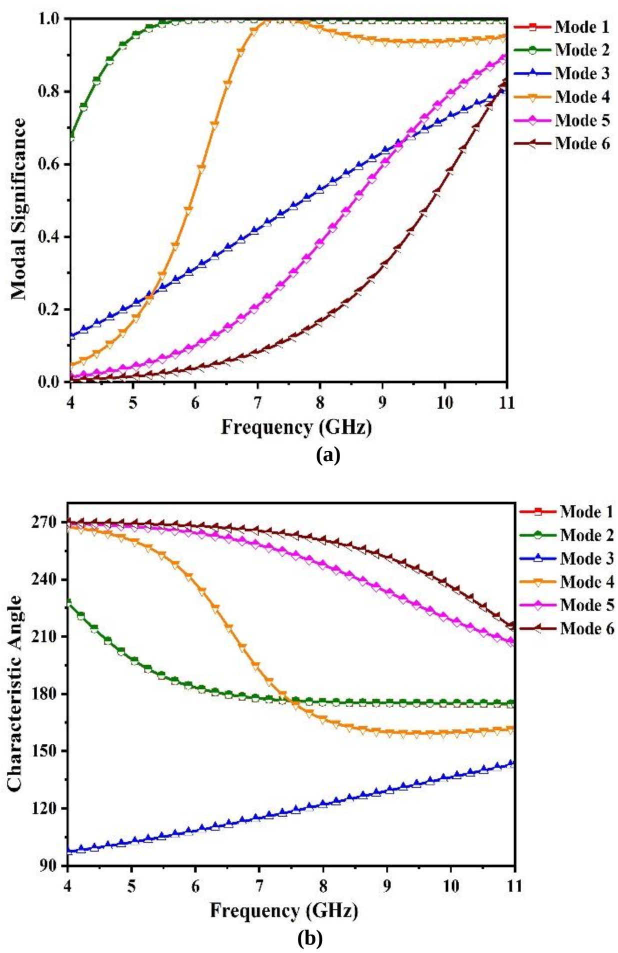

Fig. 2 Symmetric square patch #1 CM parameters (a) MS (b) CA

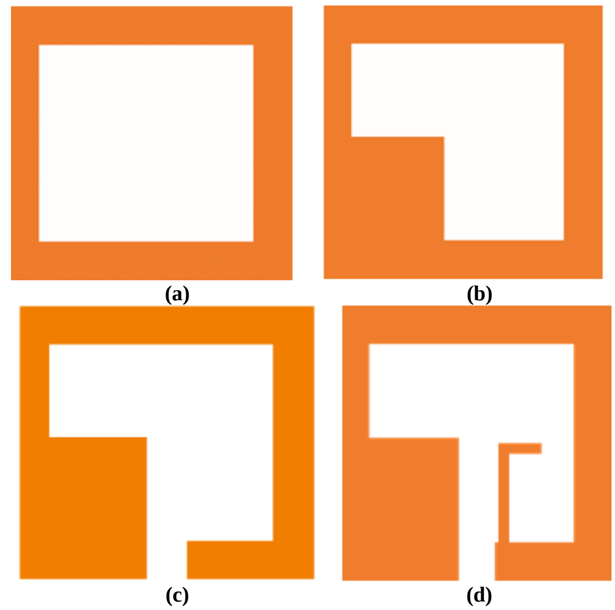

Fig. 3 Comparative analysis for patch stages. (a) Patch #2, (b) Patch #3, (c) Patch #4, (d) Patch #5

Fig. 3 illustrates various levels of modification to Patch #1. In the first level, an asymmetrical slot is added to Patch #1, resulting in Patch #2 (Fig. 3(a)). The CMs analysis of Patch #2 is depicted in Fig. 4. The results indicate that all the modes have shifted towards lower frequencies, and the degenerate modes, including Mode 1 and Mode 2, have split and resonated at two distinct frequencies. Mode 1 and Mode 2, for instance, resonate at 4.01 GHz and 4.08 GHz, respectively. More specifically, Mode 1 and Mode 2 have resonant frequencies of 4.01 GHz and 4.08 GHz, respectively. Only Mode 3 is non-resonant within the given frequency range among all six modes. Meanwhile, the higher-order modes, including Mode 4, Mode 5, and Mode 6, resonate at frequencies of 7.07 GHz, 7.87 GHz, and 11 GHz, respectively. Their combination generates a wider bandwidth with a modal suppression greater than 0.707.

During the second modification, a square patch was added to the lower left corner of the slot to create Patch #3 from Patch #2 (shown in Fig. 3(b)). The MS and CA of Patch #3 are displayed in Fig. 5. The results show that Mode 1 shifted further towards lower frequencies, and Modes 2, 4, 5, and 6 shifted slightly towards higher frequencies. Orthogonal modes from Mode 2 to Mode 6 had high MS values except for Mode 3. The frequencies where Mode 2 intersects with Mode 4, Mode 4 intersects with Mode 5, and Mode 5 intersects with Mode 6 were detected at 6.14 GHz, 8.19 GHz, and 9.84 GHz, respectively, with an MS greater than 0.7, which leads to a broader bandwidth. Moreover, at 6.14 GHz, the CA angle between Mode 2 and Mode 4 was approximately 90 degrees, accompanied by an MS value of 0.7.

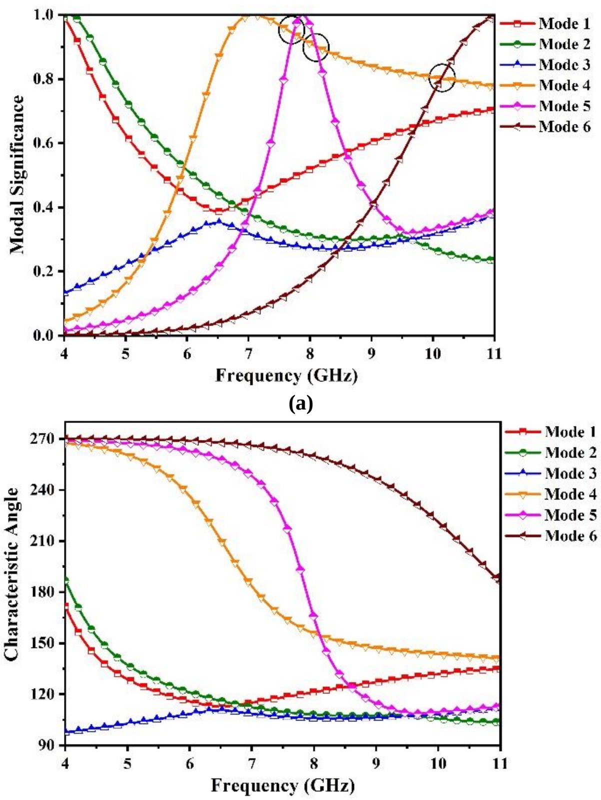

(b)

Fig. 4 Comparative analysis of characteristics modes of patch #2 (a) MS (b) CA

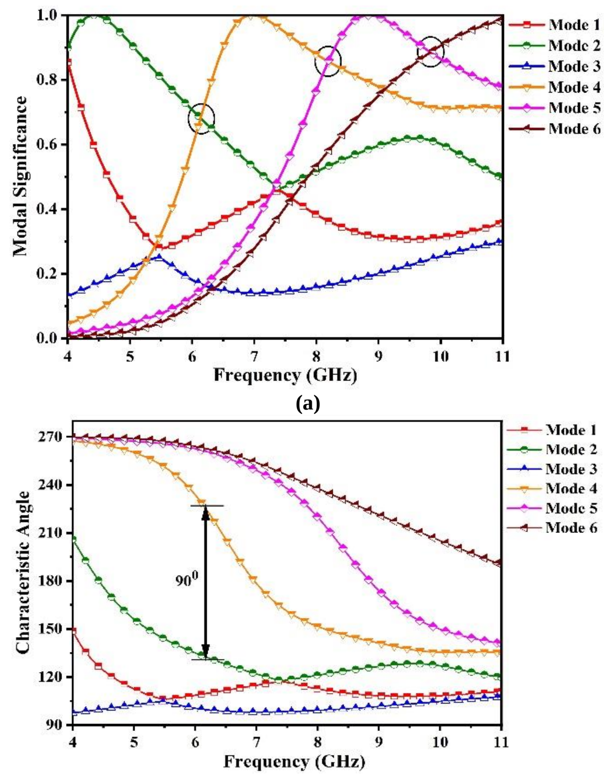

(b)

Fig. 5 Comparative analysis of characteristics modes of patch #3 (a) MS (b) CA

Patch #3 was further modified by adding a slot in the bottom center of the patch to create Patch #4 (Fig. 3(c)). The resulting MS and CA values for Patch #4 are depicted in Fig. 6. The changes to the patch caused a shift in the mode resonance frequency towards the higher frequency side and a reduction in the broader frequency band, causing Mode 2 and Mode 4 to intersect at 7.7 GHz with a phase difference of 98^0 and an MS of 0.65. To achieve a broader frequency band and shift the mode frequencies towards the lower side, an inverted L-shaped strip was added to Patch #4, as shown in Fig. 3(d), to form Patch #5. As demonstrated in Fig. 7, the addition of the strip caused a shift of all modes towards the lower frequency side, resulting in the intersection points between different modes also shifting. Mode 1 and Mode 3 became non-significant in the specified band, while the significant modes such as Mode 2, Mode 4, Mode 5, and Mode 6 contributed to the broader frequency bandwidth. Mode 2 and Mode 4 intersected at 6.19 GHz with an MS of 0.81 and a CA of 71.70, while Mode 4 and Mode 5 intersected at 8.4 GHz with an MS of 0.98 and a CA of 73.3^0. Mode 5 and 6 intersected at 9.9 GHz with an MS of 0.76 and a CA of 210, while Mode 4 and 6 intersected at 9.0 GHz with an MS of 0.76 and a CA of 77.7^0. The circularly polarized radiation is facilitated by the stable CA of approximately 70° at all intersection points, except for Mode 5 and Mode 6. This stability is beneficial for proper feeding design and an additional phase shift to generate circular polarization.

2.2. Antenna Design and Analysis

After performing a CMA analysis on the mode resonances, a square slot antenna was selected and equipped with an annular ring microstrip feed and an inverted L-strip patch to introduce a phase shift for circularly polarized radiation. The proposed design is optimized on a low-cost FR-4 substrate on 0.4 mm thickness, a relative permittivity of 4.4, and a loss tangent of 0.04. Its dimensions are $25 \times 25 \times 0.4$ mm^3, and the feed line comprises a 50 Ω transmission line with a feed length of 32.5 mm, a signal line width of 2.75 mm, and a 0.4 mm gap between the signal line and the asymmetrical slot patch. The feedline is attached to the annular ring to enhance the phase shift for circular polarization further. Fig. 8 depicts the geometric configuration of the antenna design, and Table 1 summarizes its overall dimensions.

A comparison of the simulated S11 and AR is conducted in Fig. 9 with and without an annular ring to evaluate the significance of the annular ring in the design. The results indicate that the antenna lacking an annular ring does not offer impedance matching. In contrast, the antenna with an annular ring presents a matched impedance within the frequency band from 5.41 GHz to 10.54 GHz. Furthermore, the antenna with an annular ring demonstrates improved AR, less than 3 dB, for CP radiation within the range of 5.92 GHz to 9.50 GHz.

Table 1. Geometrical parameters of the proposed antenna

Parameter	W_s	L_s	W_p	L_p	W_p	W_f	g
Value (mm)	25	25	18	18	6	2.75	0.4
Parameter	a	b	c	d	e	r_{in}	r_{out}
Value (mm)	8.3	8.5	8	1	4	2	3

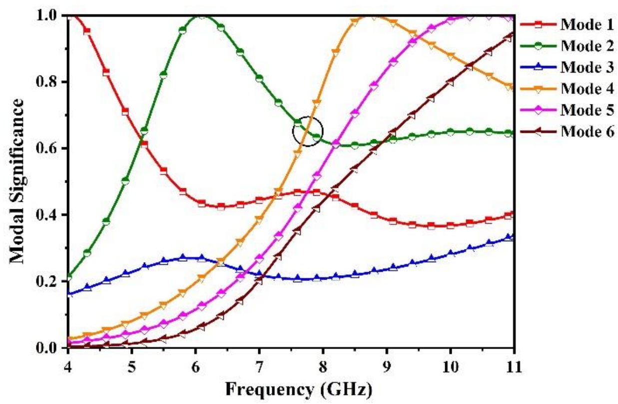

(a)

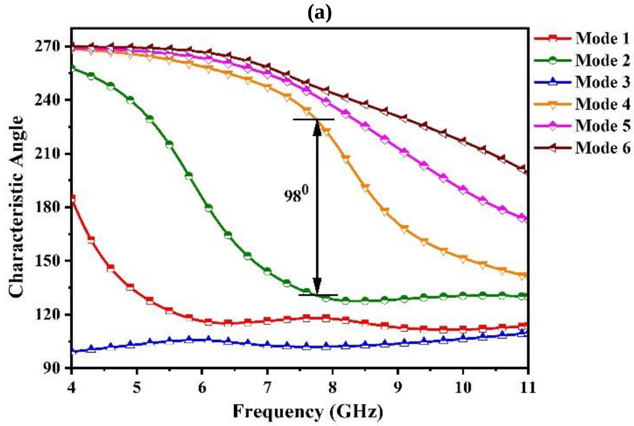

(b)

Fig. 6 Comparative analysis of characteristics modes of patch #4 (a) MS (b) CA

To investigate the IPBW and ARBW of the proposed antenna, a parametric analysis was conducted by varying the substrate thickness and feed width. The substrate thickness (h_s) analysis was performed on commercially available substrates ranging from 0.2 mm to 1.6 mm. The feed width (W_f) analysis was conducted on 2 mm to 3 mm values. The parametric thickness analysis, as shown in Fig. 10, indicates that as hs increases, the IPBW increases, and the matching shifts towards the lower frequency side. However, the ARBW becomes very poor. At 1.6 mm, the CP radiation is not provided at a certain frequency in the specified matching band. Therefore, the substrate thickness was optimized in the design to 0.4 mm to balance the IPBW and ARBW.

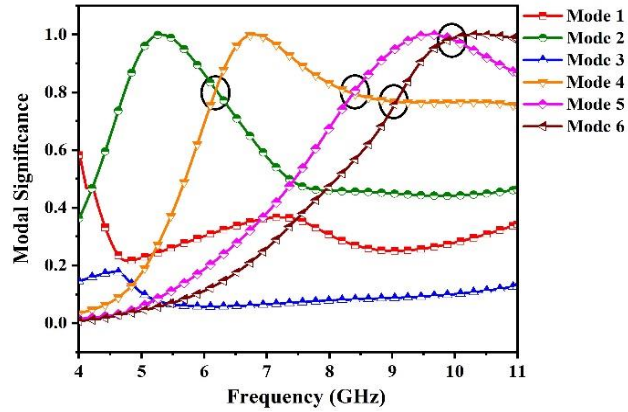

(a)

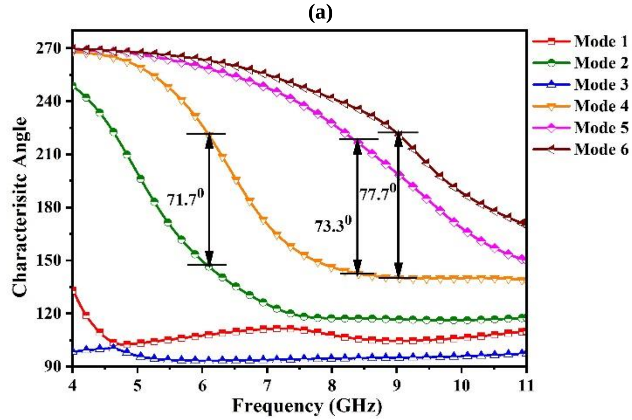

(b)

Fig. 7 Comparative analysis of characteristics modes of patch #5 (a) MS (b) CA

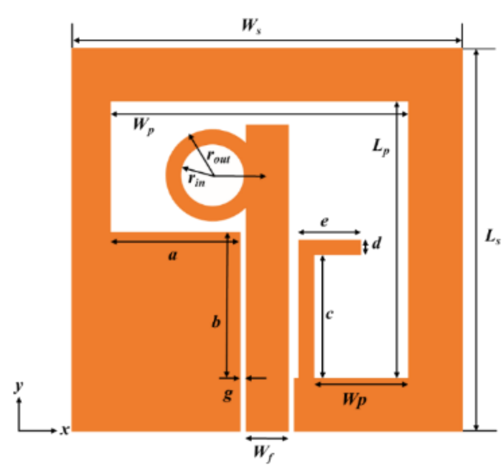

Fig. 8 Proposed CPW-Fed printed square-slot antenna design layout

The relationship between the feed width (W_f) and its variation is illustrated in Fig. 11. It is evident from the graph that there is a reduction in matching around the center frequency as the feed width is increased from 2 mm to 3 mm. This may be attributed to the need to maintain close coupling among the elements and achieve the desired ARBW and impedance matching. Furthermore, it is noted that increasing the feed width W_f results in a reduction of the ARBW, particularly at the upper-frequency edge. This could be the disturbance of soldering on the patch. Therefore, the optimal design is obtained by selecting a value of W_f that balances the IPBW and ARBW, which in this case, is 2.75 mm.

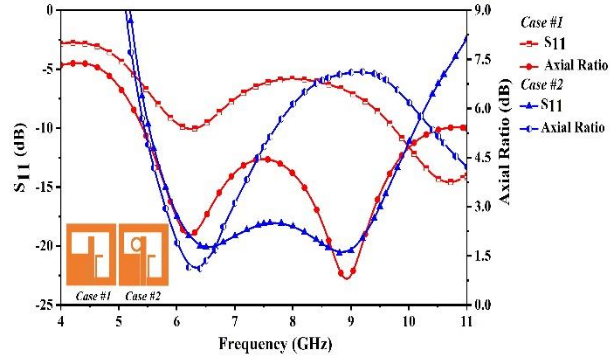

Fig. 9 Simulated S_{11} and AR plots

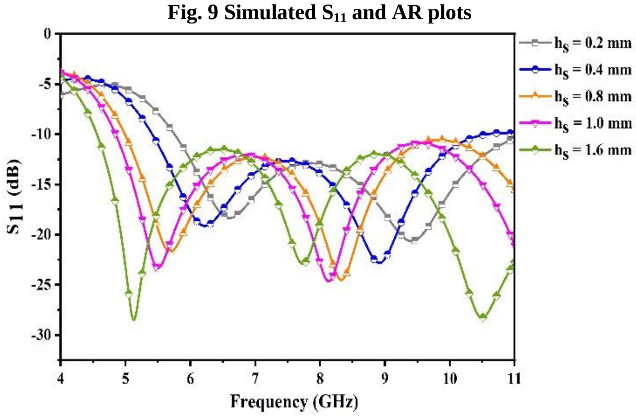

(a)

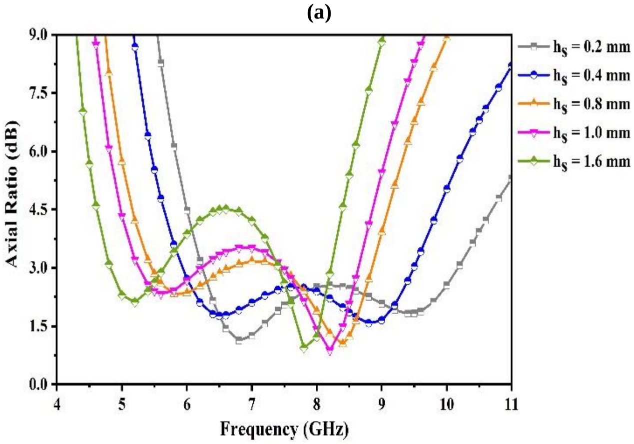

(b)

Fig. 10 Effect of variation in height (a)S_{11} (b) AR

In order to gain deeper insights into the circular polarization behavior of the antenna under consideration, an analysis of the surface current distribution is performed at a frequency of 7.5 GHz. The results, shown in Fig. 12, demonstrate surface current distribution at different phases (0^0, 90^0, 180^0, and 270^0). The current on the top left corner of the inverted L-strip asymmetrical slot patch and extended patch point rotates in an anti-clockwise direction with a 90^0-phase difference at all phase variations from 0^0 to 270^0. In addition, a clockwise current distribution is observed on the top edge intersecting point between the annular ring and feed line. These observations inferred that the antenna exhibits left-hand circular polarization.

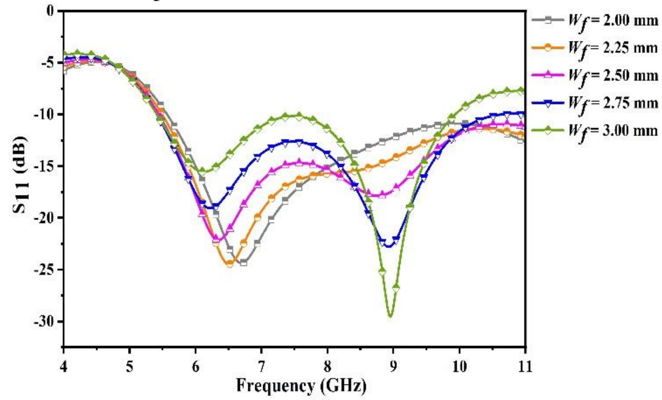

(a)

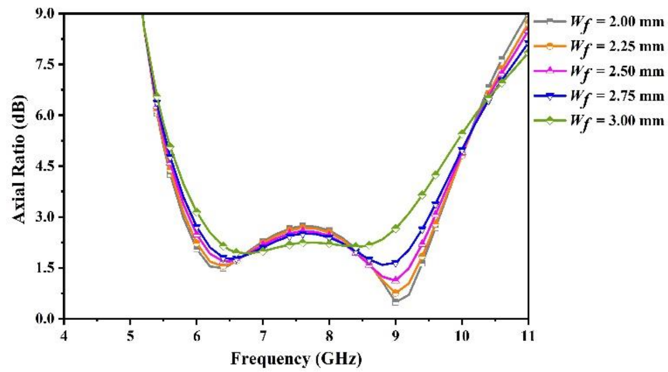

(b)

Fig. 11 Effect of variations in feed width (Wf) (a) S_{11} (b) AR plots

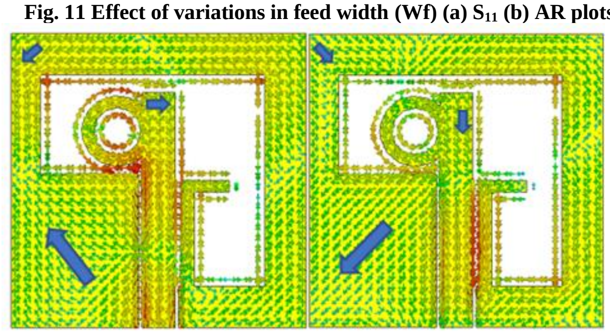

(a) **(b)**

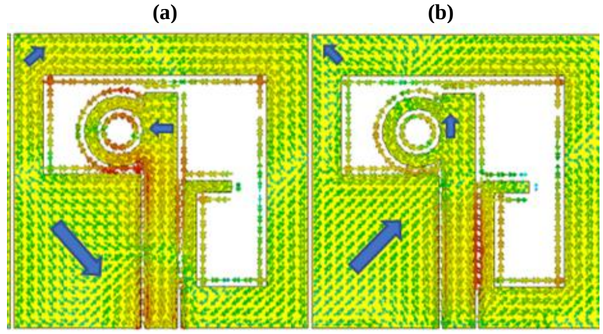

(c) **(d)**

Fig. 12 Surface current distribution of proposed antenna at 7.5 GHz. (a) $\theta = 0^0$ (b) $\theta = 90^0$ (c) $\theta = 180^0$ (d) $\theta=270^0$

2.3. Experiment Results

A prototype model is created to verify the antenna design, and various measurements are taken, such as S_{11}, axial ratio (AR), gain, and radiation pattern. The prototype is illustrated in Fig. 13(a). The S_{11} parameter is measured using the Anritsu S820E vector network analyzer. The measured S_{11} results are then compared with the simulated results, as shown in Fig.13(b). The antenna is measured IPBW is 59.6% with S_{11} of -10 dB and operates within the frequency range of 5.50 GHz to 10.17 GHz. The simulation IPBW is 64.2% within the operating band of 5.41 GHz to 10.54 GHz.

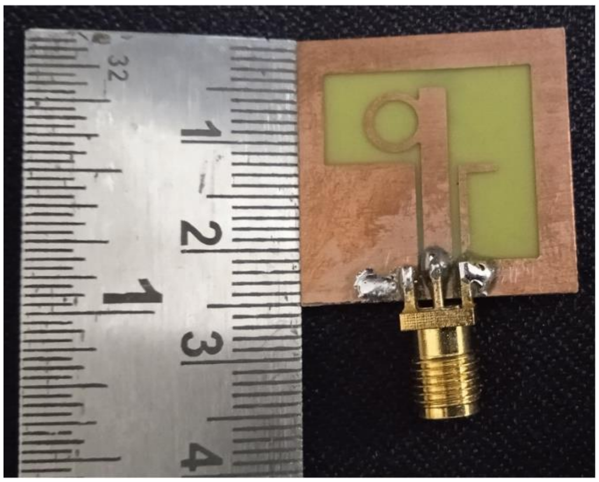

(a)

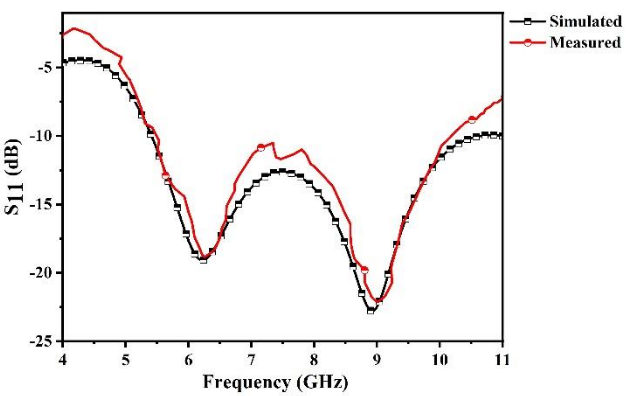

(b)

Fig. 13 (a) Antenna prototype (b) S_{11} parameter

The measured and simulated AR, along with gain plots, are shown in Fig. 14. The measured ARBW is about 46.8% (5.98 GHz to 9.64 GHz), and the simulated 3 dB ARBW is about 46.3% (5.92 GHz to 9.50 GHz). The minimum AR of the simulated and measured values is 1.57 dB (8.80 GHz) and 1.42 dB (6.58 GHz), respectively. The results indicate that both the simulated and measured values are in good agreement.

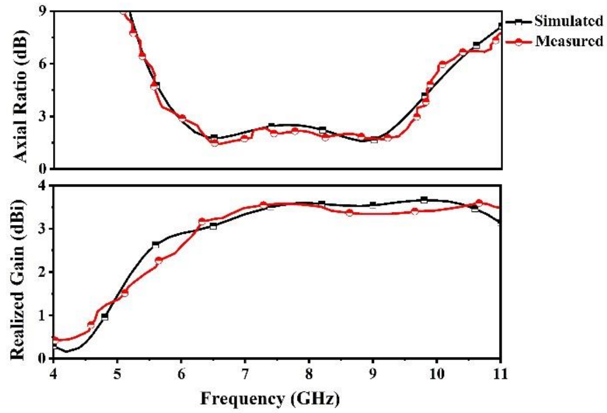

Fig. 14 Simulated and measured AR along with realized gain

Furthermore, upon measurement, it was noted that the maximum gain obtained was 3.72 dBi at 10.1 GHz. On the other hand, the simulated realized peak gain was 3.61 dBi at 10.61 GHz. The gain remains almost stable within the -10 dB IPBW and 3 dB ARBW (improving from lower to higher frequency) and starts degrading after the 3 dB AR terminating point (10.68 GHz). Table 2 provides a summary of the comparison between the measured and simulated results.

Table 2. Comparison of simulated results and measured results

Results	IPBW			ARBW		
	%	GHz	*fc*	%	GHz	*fc*
a)Sim	64.2	5.41-10.54	7.98	46.3	5.92-9.50	7.71
bMea	59.6	5.50-10.17	7.83	46.8	5.98-9.64	7.81

a) Simulated; b) Measured

The antenna's pattern is measured using an Amitech radiation pattern measurement setup, which involves placing the source antenna (horn) in the far field and mounting the measured antenna on an automated rotator with a data recorder. To exhibit the direction of circular polarization (CP), the far-field patterns are measured in both left-hand circular polarization (LHCP) and right-hand circular polarization (RHCP) at frequencies of 6.0 GHz, 7.5 GHz, and 9.5 GHz. These measured patterns are then compared to the simulated patterns in both the x-z ($\phi=0^0$) and y-z ($\phi=90^0$) planes, as illustrated in Fig.15. It is important to note that any slight discrepancies between the measured and simulated patterns may be due to fabrication defects or measurement inaccuracies.

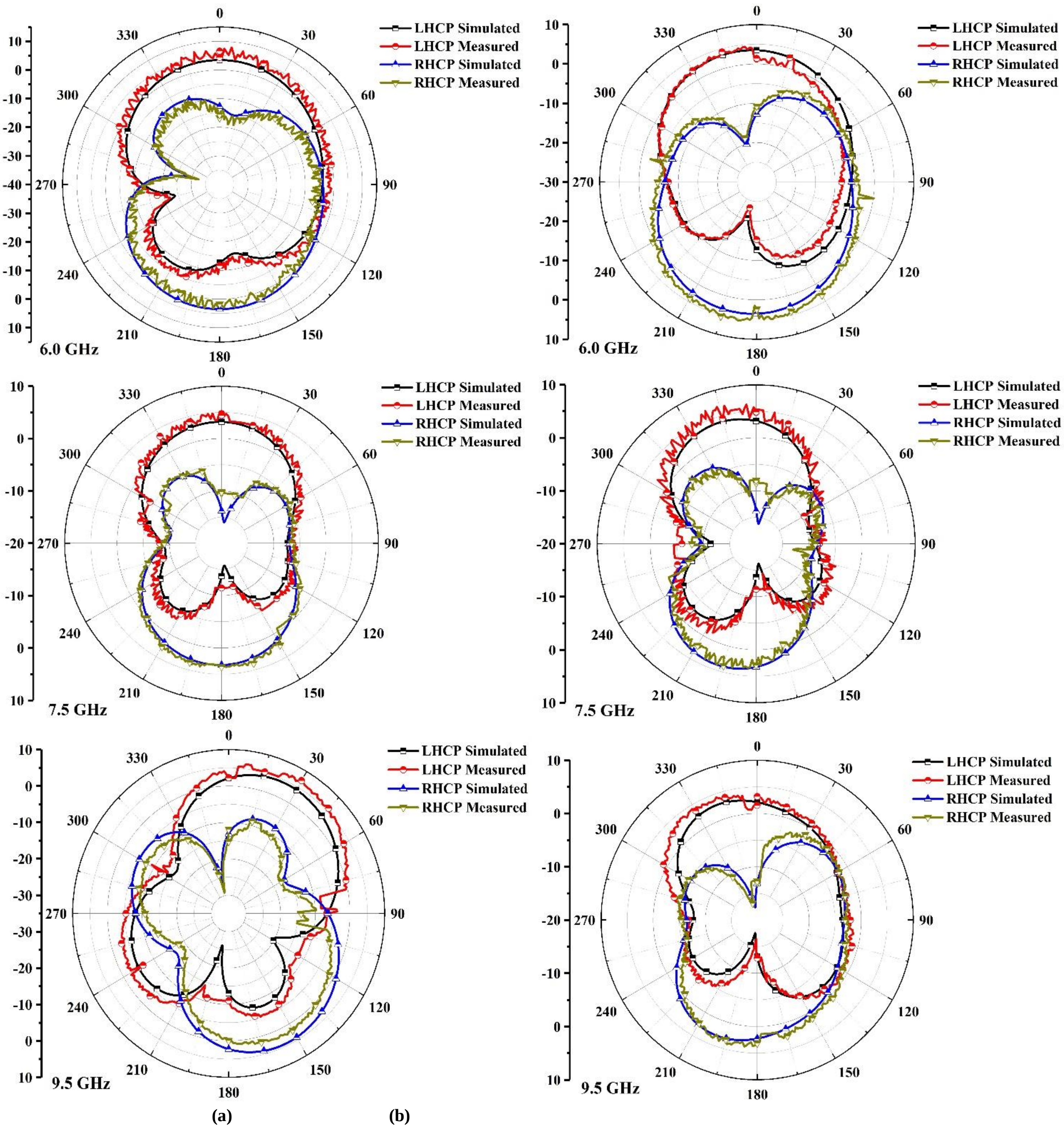

Fig. 15 Radiation pattern comparison (a) E-plane (b) H-plane

After analyzing the measured and simulated far-field patterns of the LHCP and RHCP signals at various frequencies in the x-z and y-z planes, it is found that the magnitudes of both planes are equal at their respective frequencies. Specifically, at 6.0 GHz, 7.5 GHz, and 9.5 GHz in the x-z plane, the simulated magnitude of the LHCP signal is 3.46 dBi, 3.17 dBi, and 4.25 dBi, respectively, in the main lobe direction. In contrast, the magnitude of the LHCP signal in the y-z plane is 3.53 dBi, 3.91 dBi, and 2.95 dBi in the main lobe direction at the same specified frequencies. Additionally, the difference in magnitude between the LHCP and RHCP signals is observed to be 0.03 dBi, 0.08 dBi, and 0.11 dBi in the x-z plane at 6.0 GHz, 7.5 GHz, and 9.5 GHz, respectively, in the main lobe direction at 0° and 180°.

Similarly, the magnitude difference in the y-z plane is 0.03 dBi, 0.09 dBi, and 0.11 dBi at the same frequencies. Although the RHCP component is slightly larger than the LHCP component at all frequencies, the difference is considered acceptable.

In Table 3, we compare the proposed CP antenna with the previous CP antennas. It demonstrates that this antenna has a more straightforward design, a smaller overall size, and excellent impedance bandwidths with appropriate ARBWs.

Table 3. Comparison with similar designs reported in the literature

Ref	Antenna Size w × l × h (mm)	IPBW			ARBW			Peak gain (dBi)	CMA
		%	GHz	*fc*	%	GHz	*fc*		
[26]	100×100×3	60.3	4.82-5.12	4.97	58.2	4.84-5.13	4.98	9	No
[27]	50×50×0.8	111	2.13-7.46	4.79	27.0	3.20-4.20	3.70	5.3	No
[28]	85×85×1.6	34.1	2.80-3.95	3.37	34.1	2.80-3.95	3.37	7.5	No
[29]	44.7×53×1.6	88.3	2.49-6.42	4.45	49.1	2.72-4.49	3.60	3.5	No
[30]	40×40×1.6	73.3	5.02-10.84	7.93	58.1	5.07-9.22	7.14	4.2	No
[31]	42×42×1.5	90.9	2.10-5.60	3.85	90.9	2.10-5.60	3.85	3.2	Yes
[32]	100×100×6	52.6	1.78-3.05	2.41	31.3	2.15-2.95	2.55	7.0	Yes
[33]	27×27×3.4	27.3	4.96-6.53	5.74	8.07	5.83-6.32	6.07	6.3	Yes
[34]	35×40×1.6	48.3	4.70-7.70	6.20	44.0	4.60-7.20	5.90	4.0	Yes
Proposed Work	**25×25×0.4**	**59.6**	**5.50-10.17**	**7.83**	**46.8**	**5.98-9.64**	**7.81**	**3.6**	**Yes**

3. Conclusion

In this study, the antenna structure combines a CPW-fed annular ring and an asymmetric square slot designed for broadband circular polarization (CP) using CMA. The use of CM theory offers a systematic design approach. The CP behavior is analyzed using MS and CA from CMA, and the introduction of the patch on the left bottom side and inverted L-strip of the asymmetric slot. The antenna is excited with CPW feed along with the annular ring, and good impedance matching and large ARBW are observed with the help of the annular ring compared to the antenna without it. The final proposed antenna has an overall size of 25×25×0.4 mm3 and provides an ARBW and IBW of 46.8% (5.98 – 9.64 GHz) and 59.6% (5.50 – 10.17 GHz), respectively. The effectiveness of the design technique with CMA has been validated through experimental values, which are in good agreement. The suggested broadband CP performance, simple construction, and small antenna size are appropriate for wireless C and X-band applications.

References

[1] Vamshi Kollipara, Samineni Peddakrishna, and Jayendra Kumar, "Planar EBG Loaded UWB Monopole Antenna with Triple Notch Characteristics," *International Journal of Engineering and Technology Innovation*, vol. 11, no. 4, pp. 294-304, 2021. [CrossRef]

[2] Tilak Sarmah, Pranjal Borah, and Tulshi Bezboruah, "Dual Frequency Tuning of a Microstrip Patch Antenna by Introducing Inclined Slit and Adding an Extra Portion to the Patch," *SSRG International Journal of Electrical and Electronics Engineering*, vol. 10, no. 1, pp. 15-23, 2023. [CrossRef]

[3] Samineni Peddakrishna et al., "Slot and EBG-Loaded Compact Quad Band-Notched UWB Antenna," *Iranian Journal of Science and Technology, Transactions of Electrical Engineering*, vol. 46, no. 1, pp. 205-212, 2022. [CrossRef]

[4] David M. Pozar, *Microwave Engineering*, 4th Edition, Hoboken, NJ, USA: John Wiley & Sons, 2011.

[5] Constantine A. Balanis, *Antenna Theory: Analysis and Design*, 4th Edition, Hoboken, NJ, USA: John Wiley & Sons, 2015.

[6] Mrityunjoy Kumar Ray, and Kaushik Mandal, "Pair of Diagonal Slots Loaded Low-Profile Circularly-Polarized Patch Antenna with 3-dB Axial Ration Beamwidth," *IET Microwaves, Antennas & Propagation*, vol. 13, no. 14, pp. 2433-2438, 2019. [CrossRef]

[7] May Abo El-Hassan, Khalid Fawzy A. Hussein, and Kamal H. Awadalla, "Microstrip Antenna with L-Shaped Slots for Circularly Polarised Satellite Applications," *The Journal of Engineering*, vol. 2019, no. 12, pp. 8428-8431, 2019. [CrossRef]

[8] Kollannore Ukru Sam, and Parambil Abdulla, "Axial Ratio Bandwidth Enhancement Fed Microstrip Antenna," *Progress in Electromagnetics Research C*, vol. 102, pp. 265-281, 2020. [CrossRef]

[9] Meng Zhang, Bin Li, and Xin Lv, "Cross-Slot-Coupled Wide Dual-Band Circularly Polarized Rectangular Dielectric Resonator Antenna," *IEEE Antennas and Wireless Propagation Letters*, vol. 13, pp. 532-535, 2014. [CrossRef]

[10] Abdelhady Mahmoud et al., "An Array of Staircase-Shaped Circularly Polarized DRA," *International Journal of RF and Microwave Computer Aided Engineering*, vol. 31, no. 6, pp. 1-9, 2021. [CrossRef]

[11] Gaurav Varshney, "Gain and Bandwidth Enhancement of a Singly-Fed Circularly Polarized Dielectric Resonator Antenna," *IET Microwaves, Antennas & Propagation*, vol. 14, no. 12, pp. 1323-1330, 2020. [CrossRef]

[12] Samaneh Sadeghi-Marasht et al., "A Single-Layer Circularly Polarized Planar Lens Antenna at Millimeter-Wave," *IET Microwaves, Antennas & Propagation*, vol. 16, no. 10, pp. 668-678, 2022. [CrossRef]

[13] Ki-Baek Kim, Bang Chul Jung, and Jong-Myung Woo, "A Compact Dual-Polarized (CP, LP) with Dual-Feed Microstrip Patch Array for Target Detection," *IEEE Antennas and Wireless Propagation Letters*, vol. 19, no. 4, pp. 517-522, 2020. [CrossRef]

[14] Lehu Wen et al., "Design of a Wideband Dual-Feed Circularly Polarized Antenna for Different Axial Ratio Requirements," *IEEE Antennas and Wireless Propagation Letters*, vol. 20, no. 1, pp. 88-92, 2021. [CrossRef]

[15] Pranav Bhatt et al., "Microstrip-Fed 3.04-10.77 GHz UWB Patch Antenna Design Using CMA and Parametric Study," *International Journal of Engineering Trends and Technology*, vol. 70, no. 7, pp. 250-259, 2022. [CrossRef]

[16] Chen Zhao, and Chao-Fu Wang, "Characteristic Mode Design of Wideband Circularly Polarized Patch Antenna Consisting of H-Shaped Unit Cells," *IEEE Access*, vol. 6, pp. 25292-25299, 2018. [CrossRef]

[17] Weiwen Li et al., "Modal Proportion Analysis in Antenna Characteristic Mode Theory," *International Journal of Antennas and Propagation*, pp. 1-10, 2019. [CrossRef]

[18] Ankireddy Chandra Suresh, and T. Sreenivasulu Reddy, "Design of Corona-shaped 2X2 UWB- MIMO Antenna using Characteristic Mode Analysis," *International Journal of Engineering Trends and Technology*, vol. 70, no. 3, pp. 275-283, 2022. [CrossRef]

[19] Jiang-Feng Lin, and Lei Zhu, "Low-Profile High-Directivity Circularly-Polarized Differential-Fed Patch Antenna with Characteristic Mode Analysis," *IEEE Transactions on Antennas and Propagation*, vol. 69, no. 2, pp. 723-733, 2020. [CrossRef]

[20] Vamshi Kollipara and Samineni Peddakrishna, "Circularly Polarized Antennas Using Characteristic Mode Analysis: A Review," *Advances in Technology Innovation*, vol. 7, no. 4, pp. 242-257, 2022. [CrossRef]

[21] Ranjeet Singh, and Dr. Simranjeet Singh Tiwana, "Design and Performance of a Compact Microstrip Patch Antenna using Circular Slots and Stub for RFID Applications," *SSRG International Journal of Electronics and Communication Engineering*, vol. 4, no. 8, pp. 1-6, 2017. [CrossRef]

[22] R. Garbacz, and R. Turpin, "A Generalized Expansion for Radiated and Scattered Fields," *IEEE Transactions on Antennas and Propagation*, vol. 19, no. 3, pp. 348-358, 1971. [CrossRef]

[23] Ananda Kumar Behera et al., "Fibonacci Series-Motivated Sequential-Elliptical-Pyramid Slotted Microstrip Antenna with C-Band and X-Band Isolation Features," *International Journal of Engineering Trends and Technology*, vol. 70, no. 8, pp. 118-125, 2022. [CrossRef]

[24] Yikai Chen, and Chao-Fu Wang, *Characteristic Modes: Theory and Applications in Antenna Engineering*, John Wiley & Sons, 2015.

[25] L. Magthelin Therase, and T. Jayanthy, "Metamaterial Integrated Superstrate Antenna for C, X, and Ku Bands Applications," *International Journal of Engineering Trends and Technology*, vol. 69, no. 6, pp. 38-42, 2021. [CrossRef]

[26] Yue Li, Zhijun Zhang, and Zhenghe Feng, "A Sequential-Phase Feed Using a Circularly Polarized Shorted Loop Structure," *IEEE Transactions on Antennas and Propagation*, vol. 61, no. 3, pp. 1443-1447, 2012. [CrossRef]

[27] Jen-Yea Jan et al., "Broadband CPW-Fed Circularly Polarized Slot Antenna with an Open Slot," *IEEE Transactions on Antennas and Propagation*, vol. 61, no. 3, pp. 1418-1422, 2012. [CrossRef]

[28] Mohammad Hosein Rasekhmanesh et al., "Wideband Circularly Polarized Antenna Using Sequential Phase Feed Structure and U-Shaped Radiating Patch Elements for S-Band Applications," *Microwave and Optical Technology Letters*, vol. 59, no. 11, pp. 2806-2812, 2017. [CrossRef]

[29] Jing-Li Guo et al., "A Broad Band Circularly Polarized Slot Antenna with a Compact Microstrip to CPW Transition," *International Journal of RF Microwave Computer-Aided Engineering*, vol. 28, no. 5, pp. 1-7, 2018. [CrossRef]

[30] M. Midya et al., "Pair of Grounded L-Strips Loaded Broadband Circularly Polarized Square Slot Antenna with Enhanced Axial Ratio Bandwidth," *Electronics Letters*, vol. 54, no. 15, pp. 917-918, 2018. [CrossRef]

[31] Huy Hung Tran, Nghia Nguyen-Trong, and Amin M. Abbosh, "Simple Design Procedure of Broadband Circularly Polarized Slot Monopole Antenna Assisted by Characteristic Mode Analysis," *IEEE Access*, vol. 6, pp. 78386-78393, 2018. [CrossRef]

[32] Sihao Liu, Deqiang Yang, and Jin Pan, "A Low-Profile Broadband Dual-Circularly-Polarized Metasurface Antenna," *IEEE Antennas and Wireless Propagation Letters*, vol. 18, no. 7, pp. 1395-1399, 2019. [CrossRef]

[33] Puneeth Kumar Rajanna, Karthik Rudramuni, and Krishnamoorthy Kandasamy, "Characteristic Mode-Based Compact Circularly Polarized Metasurface Antenna for in-Band RCS Reduction," *International Journal of Microwave and Wireless Technologies*, vol. 12, no. 2, pp. 131-137, 2020. [CrossRef]

[34] Wei Xu, Jingchang Nan, and Jing Liu, "Broadband Circularly Polarized Antennas with Compact Radiator Using Characteristic Mode Analysis," *International Journal of Antennas and Propagation*, vol. 2022, pp. 1-13, 2022. [CrossRef]

[35] Rohit Kumar Saini, "CPW-Fed Square Slot Antenna With Reconfigurable Circularly Polarization Characteristics for Wideband Application," *SSRG International Journal of Electronics and Communication Engineering*, vol. 8, no. 4, pp. 5-9, 2021. [CrossRef]

[36] R. J. Garbacz, "Modal Expansions for Resonance Scattering and Phenomena," *Proceedings of the IEEE*, vol. 53, no. 8, pp. 856-864, 1965. [CrossRef]

[37] Eva Antonino-Daviu et al., "Design Guidelines for the Excitation of Characteristic Modes in Slotted Planar Structures," *IEEE Transactions on Antennas and Propagation*, vol. 64, no. 12, pp. 5020-5029, 2016. [CrossRef]

[38] R. Harrington and J. Mautz, "Theory of Characteristic Modes for Conducting Bodies," *IEEE Transactions on Antennas and Propagation*, vol. 19, no. 5, pp. 622-628, 1971. [CrossRef]